# Nucleation of cubic boron nitride thin films

C. Collazo-Davila [a], E. Bengu [a,*], L.D. Marks [a], M. Kirk [b]

[a] *Materials Science and Engineering Department, Northwestern University, 2225 North Campus Drive, Evanston, IL 60208, USA*
[b] *Materials Science Division, Argonne National Laboratory, Argonne, IL 60439, USA*

**Abstract**

High-energy electrons (300 keV to 1 MeV) in a transmission electron microscope have been used to cause ballistic atomic displacements in hexagonal boron nitride. The high-resolution imaging capabilities of the TEM have allowed us to study the effect of the atomic displacements on the crystal structure of the BN. We report the formation of nanoarches — fullerene structures consisting of half of a BN nanotube capping the ends of the planar BN graphitic sheets. To form a basis of comparison between the high-energy electron bombardment and the ion bombardment typically used for cubic BN film growth, TRIM calculations were also performed to simulate $Ar^+$ ion bombardment of hexagonal BN. A model is presented, indicating a process through which the nanoarches can serve as nucleation sites for the cubic phase of BN. The nucleation model is consistent with current experimental reports on the formation of cubic BN thin films. © 1999 Elsevier Science S.A. All rights reserved.

*Keywords:* Cubic boron nitride; Electron bombardment; Ion bombardment; Nucleation; TEM

## 1. Introduction

Cubic boron nitride (c-BN), a III–V semiconductor, shares the same crystal structure as diamond and many of its attractive properties. It is extremely hard (60–70 GPa), has a high thermal conductivity (2–9 W $cm^{-1}\,K^{-1}$), and possesses a wide band gap ($\sim 6$ eV) [1]. It has been successfully doped, both p and n type, making it a strong candidate for wide-band-gap semiconducting applications. Cubic BN is also relatively inert to ferrous alloys and resistant to oxidation at elevated temperatures. Such properties make c-BN a potential material for use in UV-light-emitting diodes, high-power/high-temperature solid-state electronic devices, and wear-resistant coatings used in the steel industry.

There has been significant progress in the synthesis of nitride semiconductors in thin-film form, yet deposition of single crystal, low-defect-density c-BN thin films has not been achieved. Although polycrystalline c-BN films can be deposited using lower substrate temperatures than for diamond, the current quality of c-BN films is not good enough for commercial applications. Many questions about the nucleation and growth of

cubic BN remain unanswered. One important question, among many regarding mechanisms responsible for c-BN growth, concerns the role played by energetic ions during film evolution. It is generally accepted that some form of ion bombardment is needed during growth to form the cubic phase. It is also known that the ion bombardment creates large compressive stresses in the growing material [2] and that these compressive stresses may contribute to film adhesion problems. A combination of compressive stress and chemical attack by ambient water vapor has been blamed for cracking and delamination typically seen for c-BN films grown to a thickness of 200 nm or greater [3].

Recently, studies by McKenzie et al. [4] and Hahn et al. [5] have shown that the ion bombardment is most important during nucleation of the cubic phase. Once the nucleation step has occurred, a less severe bombardment (lower ion energy and/or flux) is capable of sustaining c-BN growth. By lowering the ion energy after c-BN nucleation took place, Mirkarimi et al. [6] were able to grow a 700 nm cubic BN film that did not delaminate from its substrate. Although this represents a significant breakthrough, 700 nm is still not thick enough for commercial applications, and the substrate temperature was kept at 800°C. Further progress is hindered by the lack of an atomic-scale understanding of the ion-induced nucleation mechanism. In order to

---

* Corresponding author. Fax: +1 847-491-7820.
*E-mail address:* bengu@apollo.numis.nwu.edu (E. Bengu)

optimize the nucleation and growth process to minimize the level of residual compressive stress, one needs an accurate model from which to gain new insight and to predict better techniques. The c-BN film formation process is a complex process with too many variables (e.g. substrate temperature, ion incidence angle, ion energy, ion mass, ion flux, boron and nitrogen flux, vacuum level, and substrate material) to expect rapid progress to be made through trial-and-error-based attempts at film growth.

The work described in this paper is an attempt toward the atomic-scale description of the ion-bombardment-induced nucleation of c-BN. The proposed nucleation mechanism is consistent with all of the experimental observations on c-BN film growth reported in the literature, and it even offers an explanation of difficulties in reproducibility which has been seen by a number of researchers working in the field.

## 2. Critical survey of current theories

There have been a large number of theoretical treatments published on c-BN film growth, and the reader is referred to Mirkarimi et al. [7] and to Kulisch and Reinke [8] for a detailed account. The aim of this section is to describe the four basic types of theories (quenching, compressive stress, subplantation, and selective sputtering) and to point out their individual strengths and weaknesses with respect to their capabilities of explaining experimental observations.

Quenching theories attribute the formation of c-BN to rapid cooling of thermal spikes caused by ion impacts. The idea of a thermal spike was first treated quantitatively by Seitz and Koehler [9]. In their treatment, an ion was modeled as depositing all of its energy as lattice vibrations at a single point in a crystal upon impact. Heat diffusion equations were then solved to find the distribution of energy as a function of time after the ion impact. It was found that for ion energies in the range of a few hundred electron-volts, a small region of the crystal a few nanometers in diameter would effectively experience temperatures of several thousand degrees for about 1 ps before the energy was dissipated. It has been argued by some researchers that the rapid quenching of the thermal spike region may allow a metastable phase to be frozen in.

Quenching models have been criticized for not being able to explain cubic BN crystal sizes of tens of nanometers, and for not offering a reason for a low-temperature boundary seen for c-BN formation. Most researchers find that c-BN film growth will not take place below approximately 100°C [7], and it is not readily apparent how a change in substrate temperature from room temperature to 100°C can play a significant role when the effective temperature in the thermal spike zone reaches several thousand degrees. However, Hofsäss et al. [10] have recently revised the calculations of Seitz and Koehler [9] with more accurate assumptions including estimating the ion energy actually transferred to lattice vibrations (which is not the ion's entire kinetic energy) and modeling the energy transfer to occur along a line in the crystal rather than at a single point. Taking 3 eV as the activation energy for an 'atomic rearrangement process', and using the phonon frequency as the rate of rearrangement attempts, Hofsäss et al. find that all of the atoms within a cylindrical volume of length equal to the ion penetration depth and with a radius of about 0.2 nm will have at least one chance to rearrange their bonding. They claim that larger crystal sizes may be easily explained by a templating effect. Once a small cylinder of the cubic phase forms, a neighboring thermal spike will solidify epitaxially on the original small grain, and eventually a large grain will build up. With respect to the low-temperature boundary seen near 100°C, Dworschak et al. [11] have argued that the temperature in the thermal spike zone should be additive with that of the substrate. Higher substrate temperatures might allow for more time before a thermal spike reaches equilibrium with its surroundings. Below a certain temperature, the spike may simply be quenched too rapidly for any c-BN to form.

In any case, one of the biggest questions about quenching is whether or not the thermal spikes are actually able to permanently rearrange any atoms at all. Mirkarimi et al. [7] claim that recent atomistic simulations of ion impacts show that melting within the thermal spike core does not occur for high-melting-point ceramics like h-BN. Also, we have performed experiments showing that 50-keV $Xe^+$ ions are not able to produce significant atomic rearrangements in h-BN at room temperature. It is well known that for metals, 50-keV $Xe^+$ ions create collision cascade volumes of about 10 nm in diameter in which substantial local concentrations of point defects are produced [12]. Amorphous volumes of similar size are produced by collision cascades in many semiconducting materials [13] and oxide superconductors [14] as well. Such small amorphous volumes or other second phases are easily visible in TEM images.

In an experiment using a high-resolution Hitachi H-9000 TEM at Argonne National Labs, a sample of h-BN was viewed in dark-field mode while simultaneously being bombarded with 50-keV $Xe^+$ ions at a dose rate of $10^{10}$ cm$^{-2}$ s$^{-1}$. Even up to a total fluence of $10^{13}$ ions cm$^{-2}$, not a single amorphous region or alternate-phase inclusion was seen. Also, the transmission electron diffraction pattern from the h-BN crystal remained sharp without any indications of disorder in the h-BN lattice. Therefore, the quenching of thermal spikes by themselves is not able to account for the formation of a new phase from h-BN. However, the

possibility of thermal spikes working in conjunction with large compressive stresses to produce a new phase cannot be ruled out.

The early compressive stress models for c-BN growth can be classified as static stress models. It is well-known that ion-induced defects lead to film densification and cause the large residual compressive stresses seen in c-BN thin films. McKenzie et al. [2] measured the compressive stress in situ during c-BN growth and found a cut-off value around 4 GPa below which no cubic BN formed. They suggested that the high pressures from the compressive stress and the high temperatures provided by thermal spikes pushed the BN into a region of its phase diagram where the cubic phase is stable. However, the previously accepted phase diagram for BN has come into question [15–17], indicating that the cubic phase may actually be the stable phase at standard temperature and pressure, and a similar investigation by Cardinale et al. [18] did not find the same sharp cut-off value of compressive stress.

Alternatively Mirkarimi et al. [19] proposed a dynamic stress model. In their model, a local instantaneous stress is determined by the steady-state production and annihilation rates of interstitials and vacancies. An additional factor describing the accumulation of defects at sinks accounts for the build-up of residual stress. They predict that the highest instantaneous stress, and hence the formation of c-BN, will take place at a depth corresponding to the maximum defect production rate. From their model, they are able to account for a critical value of momentum per depositing film atom, which has been observed experimentally [19,20].

The major shortfall of the compressive stress models is their inability to explain the effect of the substrate temperature. Higher temperatures should allow for more defect relaxation processes to occur, thus decreasing the overall dynamic or static stress. Therefore, one would expect c-BN to become more difficult at higher temperatures if compressive stress is the controlling factor, but such a trend is not observed experimentally.

Subplantation, as described in detail by Lifshitz et al. [21] to explain the growth of tetrahedral amorphous carbon (ta-C), refers to the 'shallow implantation' of ions in the energy range of 1–1000 eV. The penetration depth of an ion in this energy range will typically be a few nanometers. As the ion transfers its energy to the substrate, it displaces target atoms and causes a densification of the film with the creation of many interstitials. As the density reaches a certain critical level, a spontaneous athermal transformation to $sp^3$-bonded material takes place. Lifshitz et al. also believed that $sp^2$-bonded atoms had a lower displacement energy than $sp^3$-bonded atoms, and they claimed that the cubic phase would be favored due to a higher resistance to ion damage. This preferential displacement mechanism, however, has been refuted by measurements that indicate

that the difference in displacement energies is only around 10 eV [22,23].

As in the case of the compressive stress models, subplantation models cannot account for the substrate temperature effects found for c-BN deposition. One would again expect increased temperatures to promote the relaxation of defects resulting in a less dense film. It should be noted that subplantation does a better job at describing the growth of ta-C for which it was originally formulated. In the case of ta-C, there is no low temperature cut-off, and $sp^3$-bond formation becomes more difficult at elevated temperatures.

Proponents of the preferential sputtering model [8,24] agree that the formation of the textured t-BN layer preceding c-BN is governed by compressive stress, and they claim that the c-BN nucleation mechanism is an independent process that is not related to preferential sputtering. However, once c-BN nuclei have formed, they postulate that at a critical ion energy and flux, h-BN is preferentially sputtered to the point that the cubic phase grows more rapidly in volume than the hexagonal phase. As part of their model, they also state that an incoming atom being incorporated into the film automatically takes on the bonding hybridization of the particular phase upon which it lands. Eventually, the entire growth surface will be covered by c-BN.

To compare results from the literature, they defined the flux ratio, $F$, as the ratio of the flux of ions at the growth surface to the flux of boron atoms, and they plotted $F$ vs. ion energy, $E_{ion}$, for many different studies. They defined $F_h$ as the boundary line between h-BN formation and c-BN, and $F_c$ as the boundary between c-BN and complete resputtering of the film. At a constant temperature, they predicted the boundary lines to be proportional to the inverse sputter yield. For comparison, Reinke et al. fitted the inverse sputter yield for Si under argon bombardment to the compiled data at 500 eV and found a better agreement to the $F_h$ boundary line than for the momentum dependence predicted by Kester and Messier [20] and Mirkarimi et al. [19].

One of the strengths of the sputter model is its qualitatively correct prediction of the influence of substrate temperature over 100°C. According to Reinke et al., the effect of temperature is seen in the boron sticking probability. As the temperature is lowered, the sticking probability increases, and both $F_h$ and $F_c$ are raised. Therefore, in agreement with experiment, a higher ion flux or ion energy is needed for c-BN growth. Also, the variation of $F_h$ with the ion incidence angle as predicted by the sputter model is supported by the available studies of the effect. As $\theta$ increases ($\theta$ being measured from the surface normal), the sputter yield will increase, and $F_h$ should be lowered. Such a trend is shown in a limited study by Bouchier et al. [25] and by the work of Mirkarimi et al. [26].

The sputter model has been dealt a blow by studies

that revealed the presence of a 1- to 2-nm surface layer of $sp^2$-bonded BN sitting on top of the c-BN [25,27–30]. The mechanism of preferential sputtering clearly predicts that the growth surface should end up consisting entirely of the cubic phase. Kulisch and Reinke [8] have tried to explain the surface $sp^2$ bonding by suggesting the presence of an $sp^2$-hybridized surface reconstruction, but such a reconstruction would only involve the first layer of atoms and could not account for the estimated thickness of a few nanometers.

## 3. TEM for the study of ion bombardment effects

An accurate description of the effects of ion bombardment on BN at an atomic level is the key to understanding the formation of cubic BN thin films. In this regard, high-resolution transmission electron microscopy (HREM) is a powerful tool with its spatial resolution of $\sim 0.2$ nm. One could expect significant insight to be gained through a basic experiment in which a sample of hexagonal BN is subjected to ion bombardment and then placed into a TEM for examination. Unfortunately, such a basic experiment is made difficult by practical considerations involving the mechanical properties of h-BN and the requirements of TEM sample preparation.

Standard TEM sample preparation techniques are incapable of producing self-supporting h-BN samples with areas that are thin enough to be electron transparent. The only alternative is to support micron-sized pieces of h-BN on a fine grid structure of another material. Having a grid-supported sample does not hinder the electron microscopy in any way, but it does create problems in an ion-bombardment study. The levels of bombardment that are typically used for growing c-BN also produce a significant amount of sputtering. On a h-BN/grid sample, some of the material that is sputtered from the grid will redeposit on to the h-BN, thereby creating a contamination problem. Ion sources cannot be focused on to an individual micron-sized h-BN particle, so the sputtering problem with ions is unavoidable.

Useful experiments with h-BN samples in a TEM can still be realized, however, if one uses electron irradiation as an alternative to ion bombardment. The high-energy electron beam in a TEM can accomplish the same ballistic displacement of atoms from their lattice sites without sputtering any material from the support grid. An electron beam in a standard high-resolution TEM using a $LaB_6$ filament can be focused on to an area on the order of 1 μm across. A section of an h-BN piece away from the support grid can be subjected to intense electron irradiation, thus producing the required ballistic atomic displacements, and then the same section can be immediately imaged to record any changes occurring on an atomic scale.

The expectation that such electron irradiation experiments will be relevant to the deposition of c-BN films is supported by the literature. Boron nitride always deposits first as a textured $sp^2$-bonded layer. It is the action of the ion irradiation on this $sp^2$-bonded layer that is responsible for the nucleation of c-BN. The fact that it has not been possible to form c-BN with ion energies under 50 eV [7] is consistent with the assumption that ballistic displacements play a role of primary importance. Since high-energy electrons can produce the same ballistic displacements in h-BN, a useful insight into ion irradiation processes can be obtained.

We will examine two quantities as a basis of comparison between the ballistic displacements produced by the high-energy electron irradiations used in this study and typical ion irradiations used in c-BN growth. First, Fig. 1 shows estimated rates at which energy is transferred to the h-BN sample through elastic collisions with recoil energies above the displacement energy (taken to be 20 eV). A flux of $Ar^+$ ions with an energy of 500 eV was simulated with an amended [14] version of the program TRIM89 [31]. TRIM was used to find the distribution of vacancies produced by the ion irradiation as a function of depth into the h-BN crystal. The shape of the vacancy distribution must match the shape of the distribution of energy transferred from the ions to the h-BN lattice through elastic collisions with recoils greater than the displacement energy. Taking the incident ion energy of 500 eV, the percentage of that energy lost through collisions of 20 eV or greater (calculated by TRIM), and an ion flux of 100 μA cm$^{-2}$, the vacancy curve was rescaled to be shown in units of eV Å$^{-3}$ s$^{-1}$. It should be noted that TRIM does not take into account the crystal structure of the irradiated material, and crystal structure effects become important for ions with energies below $\sim 1$ keV. Therefore, the curve seen in Fig. 1 should be viewed with some caution. However, the values found by TRIM will not be more than a factor of 2 or 3 off, and the general form of the plot should still be useful and informative. We must also note a surface artifact arising in TRIM89 calculations, which makes the region between 0 and 0.5 nm of depth unreliable. Instead of falling to zero at the surface, the elastic energy transfer rate should intersect the vertical axis at a finite value near 1 eV Å$^{-3}$ s$^{-1}$.

In order to calculate the energy transfer rate for electron irradiations, total displacement cross-sections for boron and nitrogen atoms were estimated with the McKinley and Feshbach approximation [32] to the Mott series [33] again assuming a displacement energy of 20 eV. Two different electron irradiation conditions used in this study are graphed in Fig. 1. The inelastic mean free path of high-energy electrons in BN is much greater than the 5-nm depth shown in Fig. 1, so the energy transfer rates for electron fluxes are essentially constant and appear as straight lines. One can immediately see
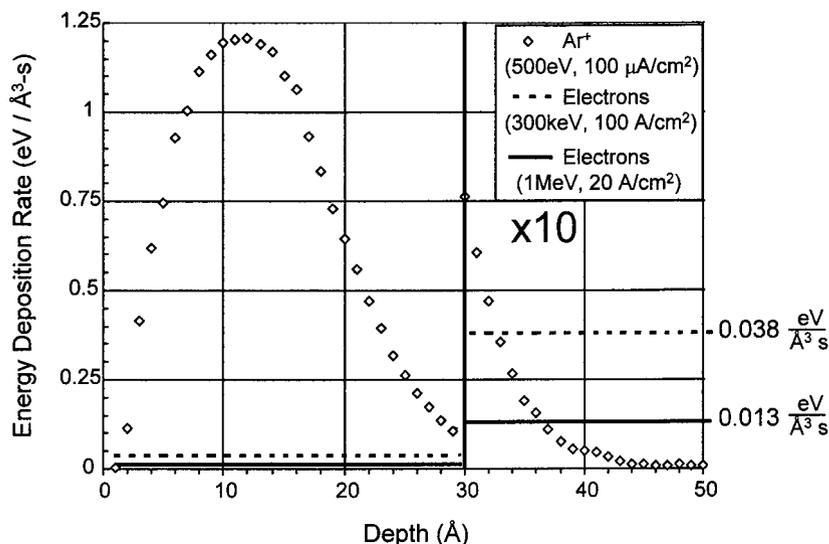
Fig. 1. Rate at which energy is transferred from a flux of ions or electrons to a h-BN crystal through elastic collisions with B or N atoms and recoil energies greater than 20 eV (the h-BN displacement energy). The data for the incident Ar$^+$ ions were simulated with amended [14] version of TRIM89 [31] software. The data for the incident electrons were calculated using total displacement cross-sections found with the McKinley and Feshbach [32] approximation to the Mott series [33].

that the energy transfer rate for the ion irradiation is much greater than the transfer rate for the electron irradiations from the surface down to a depth of about 2 nm. The two rates become comparable in magnitude at a depth of about 3 nm.

As a second quantity for comparison, we can examine the total number of displacements produced during an electron beam irradiation experiment and an ion-assisted c-BN growth run. Table 1 lists common accelerating voltages used in TEMs along with the corresponding maximum possible ballistic energy transfer from an electron to a boron or a nitrogen atom that occurs for a direct head-on collision. The estimates of the average number of displacements per atom (dpa) were calculated assuming a displacement energy of 20 eV and a 1-min exposure to an electron flux of 100 A cm$^{-2}$ ($6.24 \times 10^{20}$ electrons cm$^{-2}$ s$^{-1}$). A beam current density of 100 A cm$^{-2}$ at the sample represents an upper-range estimate of what can be achieved in a TEM with a

LaB$_6$ filament. For comparison, typical c-BN growth conditions result in an average of about five displacements per atom in the film [28]. An examination of the dpa estimates in Table 1 indicates that a similar number of ballistic displacements will be achieved for electron beam irradiations lasting about 10 min at 300 kV accelerating voltage and 100 A cm$^{-2}$ current density.

## 4. Results

Polycrystalline hexagonal boron nitride (99.5% purity) was obtained from Advanced Ceramics Corp. in the form of a sintered rod (15 cm long, 1 cm in diameter). Small flakes were scraped from the rod with a razor blade and then placed into a mortar and pestle with methanol. The h-BN flakes were crushed by hand in the methanol, and then a drop of the h-BN/methanol slurry was put on to a 1000-mesh gold grid. The methanol

Table 1
Energy transfer from electrons to boron and nitrogen atoms in a TEM

| Accelerating voltage (kV) | Boron | | Nitrogen | |
|---|---|---|---|---|
| | Max energy transfer (eV) | Estimated dpa[a] | Max energy transfer (eV) | Estimated dpa[a] |
| 1000 | 402 | 1.9 | 310 | 2.6 |
| 400 | 113 | 1.1 | 87 | 1.3 |
| 300 | 79 | 0.9 | 61 | 1.0 |
| 200 | 49 | 0.6 | 38 | 0.6 |
| 100 | 22 | 0.2 | 17 | 0.0 |

[a] The dpa values are calculated for 1 min of electron bombardment at a current density of 100 A cm$^{-2}$, assuming a displacement energy of 20 eV for both B and N. The total displacement cross-sections were calculated using the McKinley and Feshbach [32] approximation to the Mott series [33]. The modified Kinchin and Pease [34] relation was used to account for secondary displacements occurring for primary energy transfers greater than twice the displacement energy.

evaporates in minutes leaving behind micron-size h-BN pieces attached to the grid. By searching through the grid square by square in the TEM, one can find several h-BN pieces favorably oriented near a major zone axis that also have regions thin enough for HRTEM.

Fig. 2 shows high-resolution TEM images for two h-BN crystals: one viewed along the (1120) zone axis and the other along the (0001) zone. Looking along the (1120) zone, the $sp^2$-bonded sheets are parallel to the beam, and each dark lattice fringe in Fig. 2a corresponds to a single $sp^2$-bonded sheet viewed edge-on. The (0001) zone is rotated 90° with respect to (1120), and in this orientation, the $sp^2$-bonded sheets lie perpendicular to the beam. The pictures in Fig. 2a and b were taken in an UHV-H9000 TEM at an accelerating voltage of 300 kV, taking care to limit the photographed regions' exposure to the electron beam. Under normal operating conditions for HREM, the current density at the sample will be roughly 1 A cm$^{-2}$. With 300-keV electrons, a current density of 1 A cm$^{-2}$ will produce only 0.01 dpa after 1 min of irradiation (assuming a 20 eV displacement energy). The regions shown in Fig. 2a and b were not subjected to much more than 1 min of exposure to the electron beam before the images were recorded, so any ballistic displacement damage would be minimal.

The pictures shown in Fig. 3a and b are from the same areas as in Fig. 2a and b, but they were recorded after an exposure to 50–100 A cm$^{-2}$ for 10 min. The high current density was obtained by removing the condenser aperture from the beam path and adjusting the bias on the Wehnelt cup in the electron gun. These irradiation conditions will produce 5–10 dpa — a range that is comparable to the estimated 5 dpa occurring for standard ion-induced c-BN formation [28].

The structures that are seen to form with the intense electron irradiation can be referred to as nanoarches. They are essentially half-nanotubes capping the ends of the $sp^2$-bonded sheets. A model of their basic structure as viewed along the (1120) zone axis is shown in Fig. 4. The observation of the curling of $sp^2$-bonded sheets under intense electron beam bombardment is not new. The formation of onion-like structures has been reported for both carbon [35–37] and boron nitride [38]. However, the well-ordered semi-cylindrical capping seen here has only previously been reported for high-temperature/high-pressure treatments [39,40].

Before discussing the relevance of nanoarches for the nucleation of cubic BN, a few more details about their



Fig. 2. High-resolution TEM images of h-BN. (a) (1120) zone. (b) (0001) zone.
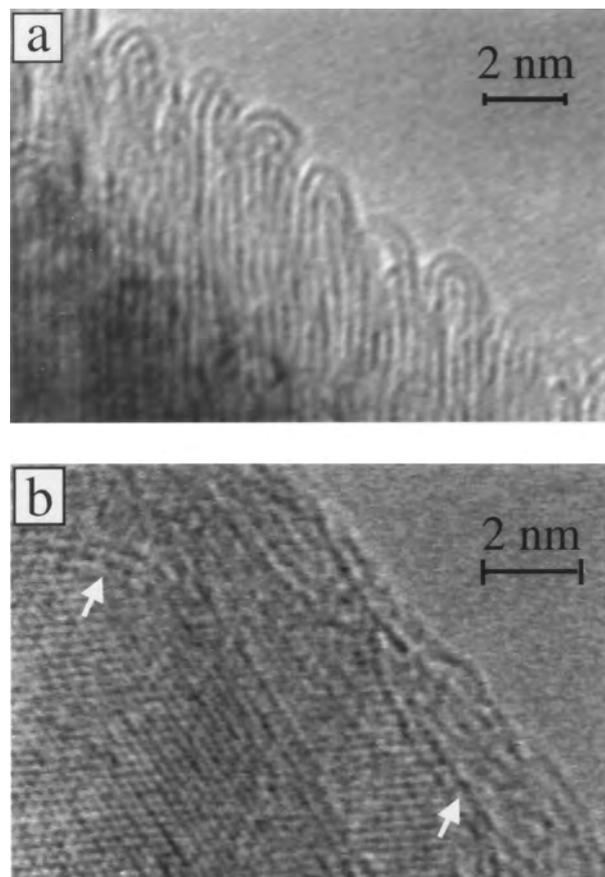


Fig. 3. Same areas that are shown in Fig. 2 after 10-min exposure to 300-keV electron beam with a current density of 50–100 A cm$^{-2}$. (a) (1120) zone. (b) (0001) zone. Arrows in (b) indicate the arches that are located at the edges of surface steps.
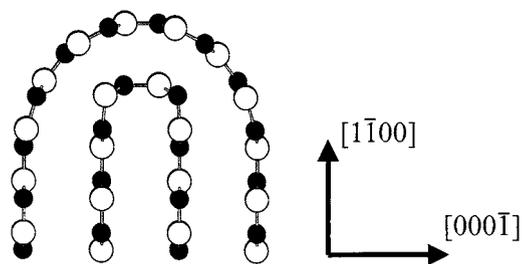
Fig. 4. Basic model of nanoarch with 1 nm diameter.



Fig. 5. Images along (1120) zone recorded on H-9000 TEM operating at a vacuum level of $\sim 5 \times 10^{-7}$ Torr. (a) Before electron irradiation. (b) Same region after 10-min exposure to 300-keV electrons at 50–100 A cm$^{-2}$ current density.

formation should be mentioned. As shown in Table 1, 300-keV electrons are capable of transferring up to 79 eV to boron atoms and 61 eV to nitrogen atoms through ballistic collisions. These values are certainly over the displacement energies for both atoms in the h-BN lattice. The electron irradiation experiments were repeated for accelerating voltages of 200 and 100 kV, and again, the BN nanoarches were seen to form. However, the arch formation rate was observed to be significantly slower for 100-keV electrons. Even with the same current density of 50–100 A cm$^{-2}$, irradiations needed to last over 30 min for large numbers of arches to form under irradiations with 100-keV electrons. Since the energy transferred to atoms through nuclear collisions decreases while the energy transferred through electronic interactions increases as the incident electron energy is lowered, a slower arch formation rate at lower electron energies suggests that the arches are created by ballistic atomic displacements rather than by electronic interactions. We can also infer some information about displacement energies in h-BN. At 100 keV, the maximum possible ballistic energy transfer has dropped to 22 eV, so at least along one crystallographic direction within the h-BN crystal, the displacement energy must be as low as $\sim 20$ eV.

Another important observation was made when the experiment was repeated in a different microscope. Fig. 5a shows a (1120) zone-axis image taken before intense electron irradiation, and Fig. 5b shows the same region just after a 10-min, 300-keV irradiation at 50-100 A cm$^{-2}$. The mottled contrast in Fig. 5b indicates that the h-BN crystal has sustained damage, but no evidence of nanoarch formation can be seen. The images in Fig. 5 were taken on a standard Hitachi H9000 TEM at Northwestern University. Apart from its base vacuum level ($\sim 5 \times 10^{-7}$ Torr), it is identical to the UHV H9000 TEM used for the images shown in Figs. 2 and 3. Longer irradiation times were tried on the standard H9000 TEM lasting up to an hour, but nanoarches could not be produced. This is in sharp contrast to the observations made with the UHV H9000 TEM, for which nanoarch formation was easily reproduced and was verified for several different samples. Further confirmation of the vacuum level dependence was obtained through experi-

ments on two other transmission electron microscopes. In another Hitachi H9000 at Argonne National Labs operating at a pressure around $5 \times 10^{-7}$ Torr, nanoarches could not be created. However, in a 1-MeV microscope in Japan operating at a pressure of $1 \times 10^{-8}$ Torr, arches could be easily formed in 20 min with irradiations of $\sim 20$ A cm$^{-2}$.
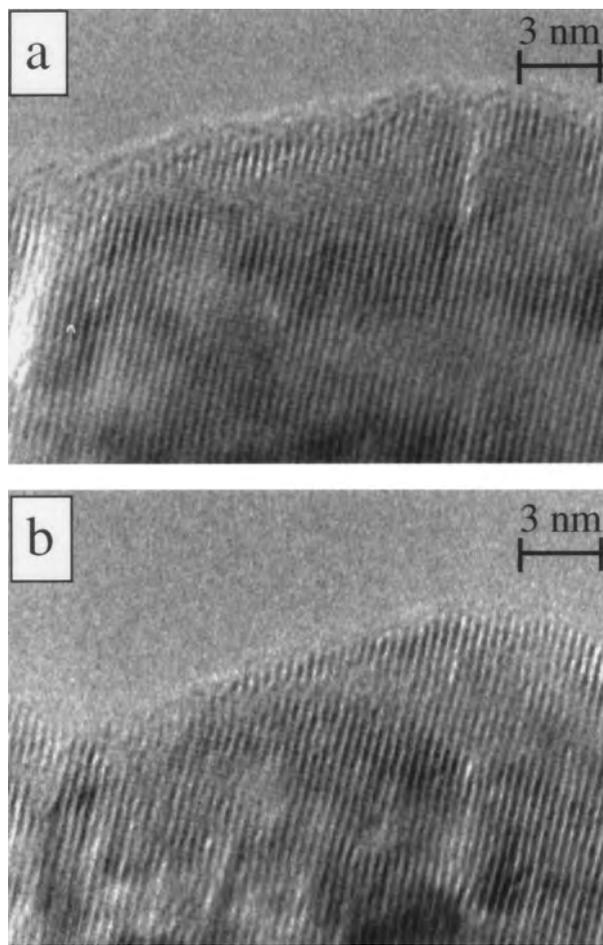
If one assumes that the driving force for the formation of the nanoarches is a reduction in the number of dangling bonds at the surface, then the difficulty in forming arches in poorer vacuum environments can be readily interpreted. Instead of the graphitic sheets creating a considerable strain energy by curling around on to themselves to saturate the dangling bonds, it is likely to be more energetically favorable for atoms from the ambient gas to bond to the edges of the sheets (e.g. termination with a single hydrogen or with an OH group). To form an arch, the edges of the sheets must be stripped free of the contaminants, and this can only be accomplished if the incident irradiation removes atoms faster than they arrive from the residual gas.

As a check for this theory, we can estimate the arrival rate of contaminant atoms in our experiments and compare it to the removal rate due to the electron bombardment. For an order-of-magnitude estimate, we can assume that the contaminant gas is $H_2$, $H_2O$, CO, or $CO_2$ and take 5 eV for the energy required to sputter a hydrogen, oxygen, or carbon atom from the surface. Then, with 300-keV electrons at a current density of 100 A cm$^{-2}$ (the conditions for the H9000 TEM experiments), each surface hydrogen, carbon, or oxygen atom will experience about 9, 13, or 15 sputtering events respectively during a 1-min time period. The arrival rate of residual gas molecules can be estimated assuming ideal gas behavior and a temperature of 300 K. With a pressure of $10^{-10}$ Torr (UHV conditions), the contaminant arrival rate is between $3.1 \times 10^{10}$ cm$^{-2}$ s$^{-1}$ for pure $CO_2$ and $1.4 \times 10^{11}$ cm$^{-2}$ s$^{-1}$ for pure $H_2$. Using the density of bonding sites available on the (1100) surface of h-BN ($1.2 \times 10^{15}$ cm$^{-2}$), the range of arrival rates can be written in a more useful form as 0.0015–0.0072 molecules per bonding site per minute. This shows that the sputtering rate is almost four orders of magnitude greater than the contaminant arrival rate, and in the steady state, the h-BN surface will be stripped almost entirely clean.

For the 1-MeV microscope in Japan operating at 20 A cm$^{-2}$, the sputtering rate was about 2, 3, or 4 per minute per hydrogen, carbon, or oxygen atom, respectively. This is to be compared with an arrival rate of 0.15–0.72 residual gas molecules per bonding site per minute ($1 \times 10^{-8}$ Torr). Since the sputtering rate is several times greater than the contaminant arrival rate, the h-BN surface sites will again be predominantly occupied by dangling bonds, and arch formation can be expected. In the case of the standard H-9000 microscopes, however, the pressure at the sample was about $5 \times 10^{-7}$ Torr. This corresponds to a contaminant arrival rate of 8–36 per bonding site per minute, which is roughly equal to the sputtering rate of $\sim 10$ per minute. It is not surprising then that arch formation does not take place, as contaminant atoms are replaced as quickly as they are sputtered.

It should be noted that these calculations are only rough estimates that include assumptions about the surface binding energy, the chemical identity of the contaminant atoms, and the contaminant sticking probability (implicitly taken as unity). Nevertheless, the binding energy estimate and the mass of the contaminant molecule are only likely to be off by at most a factor of 2 or 3, and so we can expect the order of magnitude to be accurate. The fact that the contaminant atom arrival rate is estimated to be roughly equal to the sputtering rate for a pressure near $10^{-7}$ Torr indicates that the proposed mechanism for the vacuum level influence is consistent with our experimental observations.

## 5. Significance of nanoarches for nucleation of cubic boron nitride

The creation of BN nanoarches by ballistic atom displacements reveals a direct link between ion irradiation and the nucleation of the cubic phase of boron nitride. As mentioned briefly in Section 4, the formation of nanoarches lowers the total surface energy by saturating dangling bonds at the expense of creating a significant amount of strain energy. Assuming a constant radius of curvature for an arch with a diameter of 1 nm (four sp$^2$-bonded sheets across), a B–N–B bond on the outer loop of the arch will be bent by $\sim 11°$ as projected along the [1120] direction. Eleven degrees represents a minimum estimate since some bonds will be bent to an even greater degree if the radius of curvature does not remain constant. Some experimental evidence exists for large variations in the radius of curvature for nanotubes. EELS measurements on $BC_2N$ nanotubes [41] suggested a puckered geometry for the tube walls since the B edge retained its sp$^2$-hybridized signature while the N edge indicated a relaxation towards sp$^3$ bonding.

We postulate that for nucleation of c-BN, the bond strain in the nanoarches lowers the barrier to sp$^3$ hybridization. The deposition of boron or nitrogen atoms on an arch and the formation of sp$^3$ bonds will release some of the strain energy. The addition of more B and N atoms will extend the sp$^3$ bonding network, and a small cubic BN crystal will be formed. Fig. 6 illustrates the possible steps in this cubic BN nucleation process. The structure shown in the final step (Fig. 6d) is actually modeled after the interfacial structure proposed by Widany et al. [42]. Through density-functional based tight-binding calculations, they showed that the structure was stable. It also agrees with the texture seen in c-BN thin films [basal planes in h-BN parallel to a (111) plane in c-BN]. Along the [111] direction in the cubic crystal, three cubic (111) planes match almost perfectly two hexagonal basal planes. The 5% mismatch can be easily taken up by the h-BN with its high compressibility along the [0001] direction.

## 6. Discussion

A new picture of c-BN film growth emerges based on the BN nanoarch nucleation mechanism. The film formation process is illustrated schematically in Fig. 7. First, the ion bombardment creates the textured t-BN layer (Fig. 7a) — most likely through a compressive stress mechanism. The compressive stress may even be important for compressing the sp$^2$-bonded sheets by $\sim 5\%$ to obtain a good lattice match to c-BN, but the key element for nucleation is the formation of the nanoarches (Fig. 7b). Finally, the nuclei formed through
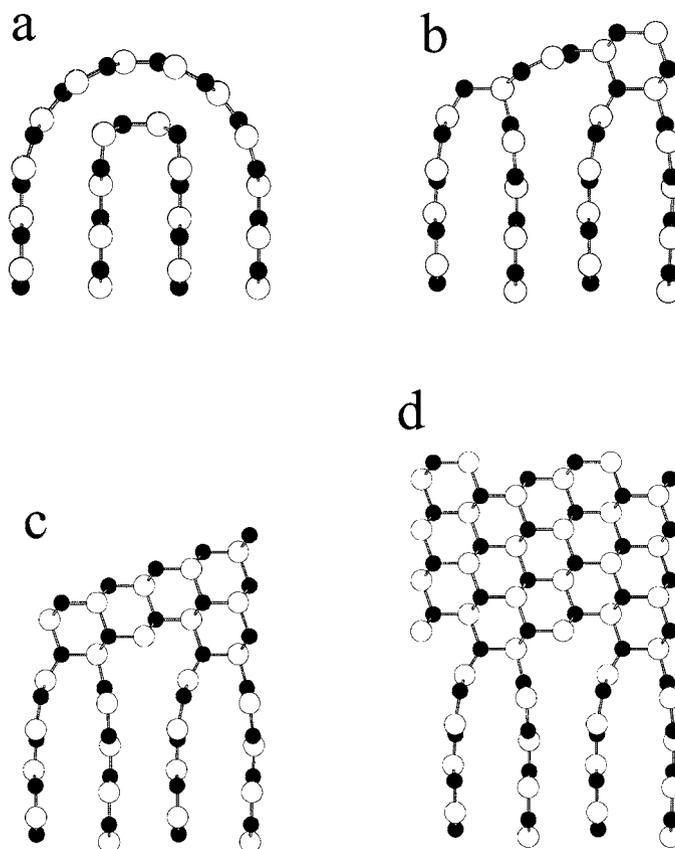
Fig. 6. Conversion of a nanoarch to a c-BN nucleus. The structure in (d) has been shown by Widany et al. [42] to be stable.
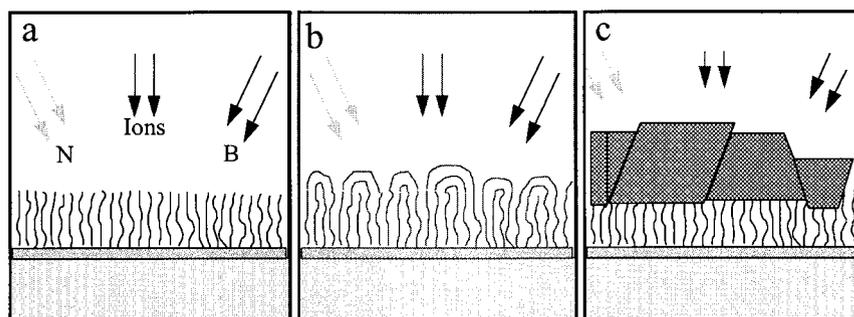


Fig. 7. Depiction of c-BN growth process based on nanoarch nucleation mechanism. (a) Formation of textured t-BN layer. (b) Formation of nanoarches. (c) Cubic BN nucleation and growth.

the nanoarches grow and coalesce, and the nanocrystalline c-BN film is formed (Fig. 7c).

This new picture of c-BN film growth is consistent with the large body of experimental evidence available on the process. Since the removal of contaminant species that is necessary for nanoarch formation is essentially a sputtering process, the correct behavior with the angle of ion incidence is predicted as in the sputter model. The correct behavior with substrate temperature over 100°C is also predicted, although the sharp cut-off in cubic phase formation below 100°C must be due to another process. The sharp temperature cut-off may occur because a threshold temperature might be required

to achieve ordering of the t-BN layer [30,43] before nanoarch formation can take place. Alternatively, the threshold temperature may be due to an instability of c-BN under ion bombardment at room temperature as seen by Ullmann et al. [44].

While further work is required to clarify the processes through which the t-BN layer becomes textured and the cubic boron nitride film continues to grow homoepitaxially after nucleation takes place, the arch nucleation model explains a number of critical growth parameters. The critical values reported for the ion energy and the ion flux are critical values needed for nucleation and therefore are well-described by the nanoarch model.

Also, while largely unpublished, a number of labs have been unable to grow c-BN, even though their deposition parameters matched those published for other workers. This irreproducibility can be attributed to the vacuum level dependence found for nanoarch formation. If the contaminant arrival rate is too high, nanoarch formation will not be possible, and the cubic phase will never nucleate.

The identification of the nucleation mechanism in cubic BN film growth opens up many new possibilities. To minimize the compressive stress, one can reduce the level of ion bombardment necessary to form c-BN nuclei by working in UHV conditions and raising the ion incidence angle to increase the sputter yield. It might also be possible to seed c-BN nucleation without ion bombardment using BN fullerene structures placed on the substrate before growth, as was demonstrated in the case of $C_{60}$ with diamond [45]. It even becomes reasonable to consider using ion-beam lithography to define c-BN structures. A thin layer of t-BN could be grown on a substrate and then a pattern could be written into it using a rastered ion beam to form c-BN nuclei only in selected areas. Of course, some of these ideas are highly speculative, but it would not even have been possible to consider them without first understanding the nucleation mechanism of c-BN on an atomic scale.

# References

[1] L. Vel, G. Demazeau, J. Etourneau, Mater. Sci. Eng. B 10 (1991) 149.
[2] D.R. McKenzie, W.D. McFall, W.G. Sainty, C.A. Davis, R.E. Collins, Diamond Relat. Mater. 2 (1993) 970.
[3] G.F. Cardinale, P.B. Mirkarimi, K.F. McCary, E.J. Klaus, D.L. Medlin, W.M. Clift, D.G. Howitt, Thin Solid Films 253 (1994) 130.
[4] D.R. McKenzie, W.D. McFall, H. Smith, B. Higgins, R.W. Boswell, A. Durandet, B.W. James, I.S. Falconer, Nucl. Instrum. Meth. B 106 (1995) 90.
[5] J. Hahn, F. Richter, R. Pintaske, M. Roder, E. Schneider, T. Welzel, Surf. Coat. Technol. 92 (1997) 129.
[6] P.B. Mirkarimi, D.L. Medlin, K.F. McCarty, D.C. Dibble, W.M. Clift, J.A. Knapp, J.C. Barbour, J. Appl. Phys. 82 (1997) 1617.
[7] P.B. Mirkarimi, K.F. McCarty, D.L. Medlin, Mater. Sci. Eng. R21 (1997) 47.
[8] W. Kulisch, S. Reinke, Diamond Films Tech. 7 (1997) 105.
[9] F. Seitz, J.S. Koehler, Solid State Phys. 2 (1956) 305.
[10] H. Hofsäss, H. Feldermann, R. Merk, M. Sebastian, C. Ronning, Appl. Phys. A 66 (1998) 153.
[11] W. Dworschak, K. Jung, H. Ehrhardt, Thin Solid Films 254 (1995) 65.
[12] H. Fukushima, M.L. Jenkins, M.A. Kirk, Phil. Mag. A 75 (1997) 1583.

[13] I. Jencic, M.W. Bench, I.M. Robertson, M.A. Kirk, J. Appl. Phys. 69 (1991) 1287.
[14] M.C. Frischherz, M.A. Kirk, J.P. Zhang, H.W. Weber, Phil. Mag. A 67 (1993) 1347.
[15] S. Nakano, O. Fukunaga, Diamond Relat. Mater. 2 (1993) 1409.
[16] V.L. Solozhenko, Termochim. Acta 218 (1993) 221.
[17] H. Sachdev, R. Haubner, H. Hoth, B. Lux, Diamond Relat. Mater. 6 (1997) 286.
[18] G.F. Cardinale, D.G. Howitt, K.F. McCarty, D.L. Medlin, P.B. Mirkarimi, N.R. Moody, Diamond Relat. Mater. 5 (1996) 1295.
[19] P.B. Mirkarimi, K.F. McCarty, D.L. Medlin, W.G. Wolfer, T.A. Friedmann, E.J. Klaus, G.F. Cardinale, D.G. Howitt, J. Mater. Res. 9 (1994) 2925.
[20] D.J. Kester, R. Messier, J. Appl. Phys. 72 (1992) 504.
[21] Y. Lifshitz, S.R. Kasi, J.W. Rabalais, W. Eckstein, Phys. Rev. B 41 (1990) 10468.
[22] H.J. Steffen, D. Marton, J.W. Rabalais, Phys. Rev. Lett. 68 (1992) 1726.
[23] J. Koike, D.M. Parkin, T.E. Mitchell, Appl. Phys. Lett. 60 (1992) 1450.
[24] S. Reinke, M. Kuhr, W. Kulisch, R. Kassing, Diamond Relat. Mater. 4 (1995) 272.
[25] D. Bouchier, G. Sene, M.A. Djouadi, P. Moller, Nucl. Instrum. Meth. B 89 (1994) 369.
[26] P.B. Mirkarimi, D.L. Medlin, K.F. McCarty, J.C. Barbour, Appl. Phys. Lett. 66 (1995) 2813.
[27] T.A. Friedmann, P.B. Mirkarimi, D.L. Medlin, K.F. McCarty, E.J. Klaus, D.R. Boehme, H.A. Johnsen, M.J. Mills, D.K. Ottesen, J.C. Barbour, J. Appl. Phys. 76 (1994) 3088.
[28] G. Sene, D. Bouchier, S. Ilias, M.A. Djouadi, J. Pascallon, V. Stambouli, P. Moller, G. Hug, Diamond Relat. Mater. 5 (1996) 530.
[29] K.S. Park, D.Y. Lee, K.J. Kim, D.W. Moon, Appl. Phys. Lett. 70 (1997) 315.
[30] H. Hofsäss, H. Feldermann, M. Sebastian, C. Ronning, Phys. Rev. B 55 (1997) 13230.
[31] J.P. Biersack, L.G. Haggmark, Nucl. Instrum. Meth. 174 (1980) 257.
[32] W.A. McKinley, H. Feshbach, Phys. Rev. 74 (1948) 1759.
[33] N.F. Mott, Proc. R. Soc. Lond. A 124 (1929) 425.
[34] G.H. Kinchin, R.S. Pease, Rep. Prog. Phys. 18 (1955) 1.
[35] D. Ugarte, Nature 359 (1992) 707.
[36] F. Banhart, P.M. Ajayan, Nature 382 (1996) 433.
[37] L.C. Qin, S. Iijima, Chem. Phys. Lett. 262 (1996) 252.
[38] F. Banhart, M. Zwanger, H.J. Muhr, Chem. Phys. Lett. 231 (1994) 98.
[39] S. Horiuchi, L.L. He, M. Akaishi, Jpn. J. Appl. Phys. 34 (1995) L1612.
[40] L. Boulanger, B. Andriot, M. Cauchetier, F. Willaime, Chem. Phys. Lett. 234 (1995) 227.
[41] Z.. Weng-Sieh, K. Cherrey, M.G. Chopra, X. Blase, Y. Miyamoto, A. Rubio, M.L. Cohen, S.G. Louie, A. Zettl, R. Gronsky, Phys. Rev. B 51 (1995) 11229.
[42] J. Widany, T. Frauenheim, W.R.L. Lambrecht, J. Mater. Chem. 6 (1996) 899.
[43] K.F. McCarty, P.B. Mirkarimi, D.L. Medlin, T.A. Friedmann, J.C. Barbour, Diamond Relat. Mater. 5 (1996) 1519.
[44] J. Ullmann, J.E.E. Baglin, A.J. Kellock, J. Appl. Phys. 83 (1998) 2980.
[45] R.J. Meilunas, R.P.H. Chang, S. Liu, M.M. Kappes, Appl. Phys. Lett. 59 (1991) 3461.